Circularly Polarized Antennas Using Characteristic Mode Analysis: A Review

Vamshi Kollipara, Samineni Peddakrishna[*]

School of Electronics Engineering, VIT-AP University, Amaravati, India

Abstract

Characteristic mode analysis (CMA) can be used in antenna designs to solve radiation problems. This review focuses on the existing development methodologies for circularly polarized (CP) antennas and their axial ratio bandwidth (ARBW) improvement using CMA. To discuss the physical insights related to CP radiation, this study systematically examines different antenna design structures used in previous research. It investigates the impact of modal parameters such as the eigenvalue, modal significance (MS), characteristic angle (CA), surface current, far-field radiation behavior on CP radiation, and ARBW for various antenna designs. In addition, it discusses the comparative analysis of various antenna design approaches in terms of antenna performance parameters such as the operating frequency band, ARBW, and gain. The results show that CMA provides more valuable information for the selection of feed position in antenna designs than the conventional full-wave simulation approach.

Keywords: characteristic mode analysis (CMA), eigenvalues, modal significance, characteristic angle

1. Introduction

Today's advanced wireless communication technology development is being driven by different integrated challenges. The antenna design methodology is one of the interesting challenges with desired radiation behavior [1-3]. An independent antenna design approach contributes to the optimization of a communication system [4-5]. Sometimes, in such a communication system, unnecessary power losses may occur if the polarization of the receiving and transmitting antennas is not matched. By using circularly polarized (CP) antennas, power losses due to polarization mismatch can be avoided. CP antennas are essential in various applications due to their ability to combat multi-path interference and mitigate linear polarization (LP) problems such as Faraday rotation [6]. CP radiation can be achieved by combining two orthogonal LP radiations with equal magnitude and quadrature-phase excitations. Additionally, various techniques have been used, such as adjusting patch shapes with single or multiple feed networks through parameter sweeping [7] and using automated optimization methods [8].

Most of the antenna designs typically follow a cut-and-try approach, based on the engineering experience by full-wave simulation without understanding the natural resonance characteristics of structures. This procedure becomes somewhat trivial and lacks physical insights. Because of this, the final simulation characteristics such as the radiation efficiency, input impedance, and radiation patterns of antennas are dependent on the resonance properties themselves from the exciting external feed. Hence, the antenna resultant current distribution does not reflect the natural resonance characteristics with the improper feed. Thus, to understand and analyze the resultant current distribution that does reflect the natural resonant behavior, the theory of characteristic mode analysis (CMA) is one of the fundamental approaches of recent days in the antenna domain. CMA analyzes the resonant behavior of an antenna structure using a source-free method and it decomposes the full-wave current into an individual mode [9-10]. This will help understand the physical insights and optimal feed arrangements, and excite the desired modes by suppressing undesired modes [11]. The optimization can thus be done on the designs to the desired radiation performance.

---

[*] Corresponding author. E-mail address: krishna.samineni@gmail.com

CMA was originally addressed by Garbacz [12] and formulated with Turpin [13]. They demonstrated a specific set of characteristic modes (CMs) for an arbitrary perfect electric conductor (PEC) obstacle that is independent of any specific source. There is only the assumption that CMs have been given instead of an explicit definition. Therefore, Harington and Mautz [14] refined the CM theory for PEC objects by relating the surface current to the tangential electric field and defined that an infinite number of independent current modes can naturally exist in an arbitrary structure. Later, it has been extended to different structures [15-16]. However, the appropriateness of their formulations has not been exhibited properly in solving practical problems.

In recent years, numerous investigations into these earlier formulations have been addressed [17-19]. The most important applications of these findings include mobile handset antenna designs [20], radio-frequency identification (RFID) tag antennas [21], universal serial bus (USB) dongle antennas [22], aircrafts [23], unmanned aerial vehicles (UAV) [24-25], ships [26], and land vehicles [27-29]. Recently, the study has been extended to a dual-port fractal ultrawideband (UWB) multiple-input multiple-output (MIMO) antenna for portable handheld wireless devices [30] and a 4-port MIMO antenna for 5.8 GHz WLAN applications [31]. Very recently, some 5G antennas have also been proposed using MIMO technology [32-36]. The CM theory has become a standard approach in these developments.

In this article, the authors explore the CM-based methodological advancement for a variety of critical CP antenna designs. This article intends to assemble and organize the advanced research achievement made in the area of CM studies, especially for the CP achievement with wide axial ratio bandwidth (ARBW). It gives preliminary knowledge about the CM parameters and helps readers get a deeper understanding of various practical antenna developments using CM-based methodologies. The organization of the article is in the following manner. Section 2 explains the basic CM parameters that are required for understanding the natural resonance behavior of an antenna. Section 3 describes the comprehensive methodologies in the literature for the CP achievement and ARBW enhancement using CMA. Section 4 concludes the discussion followed by a list of references.

2. CM Parameters

This section discusses the formulation of CMs and their parameters that are useful in antenna designs. The initial phase of any antenna design using CMA involves the modal analysis. This will help understand the modal behavior of geometry. Mathematically, it can be thought of as eigenvalue analysis [37]. Typically, CMA begins by extracting the resonance information from CM parameters. These CM parameters are obtained by solving an eigenvalue equation that is derived from the method of moment impedance matrix as shown in Eq. (1) [13].

$$[Z] = [R] + j[X] \tag{1}$$

From this, an eigenvalue equation is formulated as Eq. (2):

$$[X][I]_n = \lambda_n [R][I]_n \tag{2}$$

Here, X and R are the imaginary and real parts of the generalized impedance matrix $[Z]$, respectively. Vector I_n is the eigen or characteristic current, where n represents the index of each mode. λ_n is the real eigenvalue. This represents the possible modes that are naturally supported by the structure. By observing the real eigenvalue λ_n, the physical insight corresponding to the natural resonance information is obtained.

2.1. Eigenvalue (λ_n)

An eigenvalue (λ_n) provides useful information about the natural resonant frequency of an intended antenna design, especially as a function of frequency. The eigenvalue is useful to identify the mode information because its magnitude is proportional to the total stored field energy within a radiating antenna. Based on the stored electric and magnetic energy, the associated mode information can be classified as resonant mode, inductive mode, and capacitive mode.

In particular, if it shows $\lambda_n = 0$, i.e., the stored magnetic energy is the same as the stored electric energy as represented by Eq. (3), the associated modes are said to be resonant.

$$\iiint\limits_V = \mu H_n . H_n^* dV = \iiint\limits_V \varepsilon E_m . E_n^* dV \tag{3}$$

If it shows $\lambda_n > 0$, i.e., the stored magnetic energy is more than the stored electric energy as represented by Eq. (4), the associated modes are said to be inductive.

$$\iiint\limits_V = \mu H_n . H_n^* dV > \iiint\limits_V \varepsilon E_m . E_n^* dV \tag{4}$$

If it shows $\lambda_n < 0$, i.e., the stored magnetic energy is less than the stored electric energy as represented by Eq. (5), the associated modes are said to be capacitive [6].

$$\iiint\limits_V = \mu H_n . H_n^* dV < \iiint\limits_V \varepsilon E_m . E_n^* dV \tag{5}$$

To understand the behavior of eigenvalues for various modes supported by the structure, a typical rectangular patch with 25×160 mm is considered to represent the eigenvalues for various modes [38]. As can be seen from Fig. 1, the eigenvalues of mode 1 and mode 4 are approaching zero, and these modes are identified as resonance frequencies across the frequency band. In addition, it shows the sign of the eigenvalue of mode 3 indicating the ability to store electrical energy ($\lambda_n < 0$) and mode 2 indicating the ability to store magnetic energy ($\lambda_n > 0$). However, if higher frequencies are considered with higher-order modes, more than one mode turns into the resonance conditions. Hence, for good polarization purity, it is not easy to excite a single mode. Also, extracting the modal resonance properties for higher frequencies becomes quite difficult because they are tightly grouped and cannot be differentiated from each other. Therefore, to visualize those resonating characteristics, additional parameters such as modal significance (MS) and characteristic angle (CA) are defined along with eigenvalues.
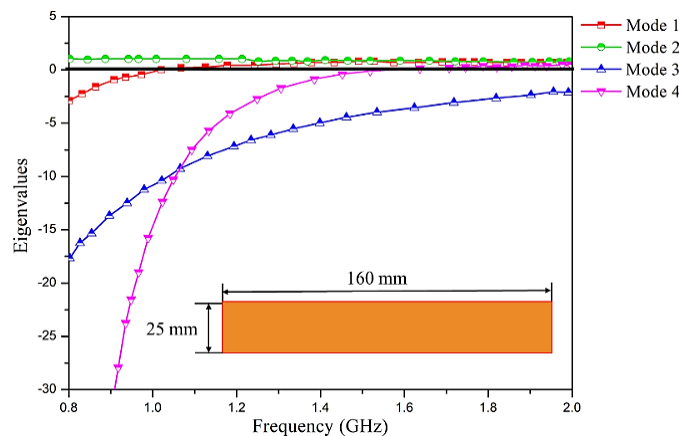

Fig. 1 Variation of eigenvalues for different modes [38]

2.2. *Modal significance* (*MS*)

MS is another way of extracting the resonance characteristics by using eigenvalues, and it measures the potential contribution of each mode. MS is the intrinsic property of each mode and is defined in Eq. (6):

$$MS = \frac{1}{|1 + j\lambda_n|} \tag{6}$$

From Eq. (6), it can be observed that the eigenvalue λ_n tends to be zero, and the MS becomes one and the mode starts resonating. The MS range transforms to [[0, 1]] from the much higher eigenvalue range $[-\infty, +\infty]$. Therefore, in many cases, to investigate the resonant behavior, it is more convenient to use MS than eigenvalues, especially over wide frequency band applications. Additionally, MS is also used to determine how many significant modes will be considered in the antenna design from the contribution of eigenvalues. To distinguish the significant modes and non-significant modes, the half-power MS is defined. From this, if MS $\geq$ 0.707, the associated modes are significant. If MS < 0.707, the associated modes are non-significant. Further, the half-power MS also reinforces the definition of each CM bandwidth, especially in the case when the feed structure is not available in the initial stage of the design. The half-power bandwidth of each CM is defined in Eq. (7).

$$BW = \frac{f_H - f_L}{f_{res}} \tag{7}$$

where f_{res}, f_H, and f_L are the resonant frequency, upper half frequency, and lower half frequency, respectively. They are determined from Eq. (6) in the following manner. If $\lambda_n = 0$ and MS = 1, then the associated mode is a resonant mode (f_{res}). If $\lambda_n = \pm 1$ and MS = 0.707, then the associated mode is the lower and upper half power frequency band mode (f_L and f_H), as shown in Eq. (8):

$$MS(f_L) = MS(f_H) = \left| \frac{1}{1 + j\lambda_n} \right| = \frac{1}{\sqrt{2}} = 0.707 \tag{8}$$

As a further extension, Fig. 2 shows the associated MS behavior of each mode supported by the same structure across the frequency for four different modes [38]. As observed from the figure, MS approaches unity for mode 1 and mode 4 and is considered to contribute to the radiation. Mode 2 and mode 3 are considered non-significant modes.
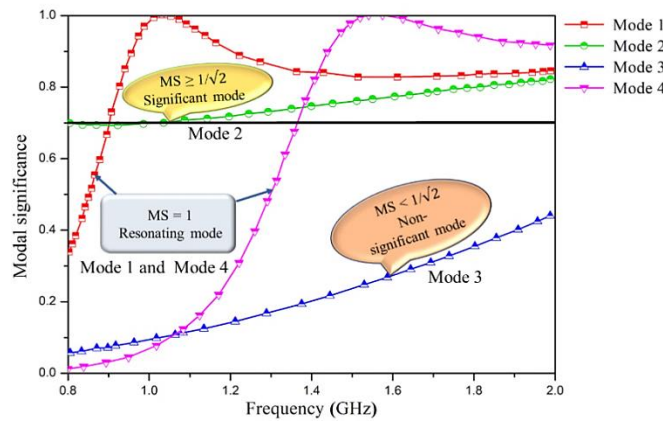

Fig. 2 Variation of MS for different modes [38]

2.3. Characteristic angle (CA)

CA is another way to show the mode behavior near resonance. It is the phase lag between the real characteristic current on the surface and the tangential electric field. This can be extracted from the eigenvalue using Eq. (9).

$$\varnothing_n = 180° - \tan^{-1}(\lambda_n) \tag{9}$$

From Eq. (9), if $\lambda_n = 0$, the phase lag between the electric field and real current on the surface is 180° out of phase, and the mode is said to be the most effective radiating mode of the radiating element. On the opposite, if $\lambda_n = \pm\infty$, the attained phase lag is 90° or 270°, and the mode is said to be non-radiating or cavity resonance mode [9]. In this case, the modal current generates a null field in the exterior region. Additionally, if the phase angle varies between [90°, 180°] and [180°, 270°], the modes are said to be inductive modes and capacitive modes, respectively.

To further understand the associated modal behavior of each mode supported by a structure, the variation of CA across the frequency for four different modes is shown in Fig. 3 [38]. From the figure, it can be easily understood that the variation of CA for mode 1 and mode 2 attains 180° phase lag at a certain frequency and these are considered resonant modes. Mode 3 and mode 4 are varying between [90°, 180°] and [180°, 270°] over a given frequency range, so they are said to be inductive modes and capacitive modes, respectively.
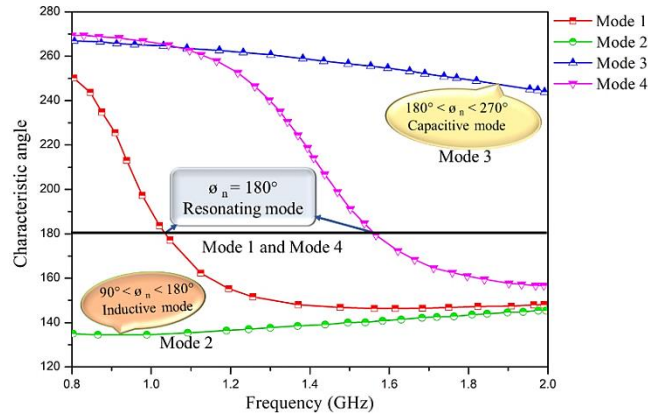

Fig. 3 Variation of CA for different modes [38]

2.4. Eigen current or field

In addition to the characteristic parameters, the real eigen currents are important to illustrate various possible currents or fields that are naturally supported by the structure. Thorough investigations into modal currents and modal fields can yield useful information on how to feed the structure for certain desirable radiation patterns. To excite the desired mode, a source needs to be positioned at a location with high characteristic currents. To understand how to place the source to excite all of the desired CMs from the characteristic currents, the modal currents of the first three normalized modes are illustrated in Fig. 4 [39]. As from the current distribution, the maxima and minima of the individual CMs J_1, J_2, and J_3 are primarily observed at the edges of the major and minor axis and can be characterized by a sinusoidal behavior. As regards this current behavior, two feeding methods have been proposed: the capacitive coupling element (CCE) and inductive coupling element (ICE) methods. For efficient mode excitation, CCE and ICE have to be placed at the location with the minimum and maximum characteristic current, respectively.

(a) Surface current and field   (b) Sinusoidal behavior of current
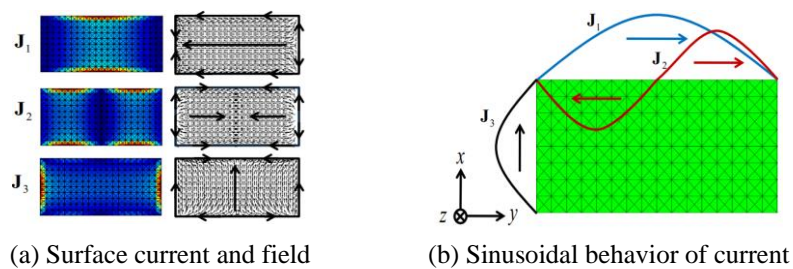Fig. 4 Modal current and field pattern variation [39]

However, practical radiating antennas typically consider the effect of source excitation. From the source excitation point of view, modal decompositions can tell how well each of the designs is excited in the desired modes. This can be done by calculating the quantities called modal excitation coefficient (MEC), modal weighting coefficient (MWC), and modal input power from Eqs. (10)-(14). The total current on the structure is assumed to be linear superposition of the orthogonal set of mode currents [14, 37]. This can be extracted from Eq. (10).

$$J_{tot} = \sum_{n}^{\infty} C_n . J_n \tag{10}$$

where C_n is the MWC and J_n is the characteristic current of the mode n.

MWC is an important guiding parameter for an antenna design to determine the appropriate feed point and feed structure telling which mode carries the maximum current.

$$| C_n | = \frac{1}{| 1 + j\lambda_n |} \cdot | \int J_n.E_i dS |$$ (11)

$$| C_n | = MS. | v_n |$$ (12)

where v_n is the MEC which describes an easy way to excite the mode from its excitation.

$$| v_n | = \int J_n.E_i dS$$ (13)

From Eq. (12), it can be understood that a large MS and MEC are necessary to excite the desired operating modes. Another important parameter is the modal input power, which is described as the power in each mode and used to find which mode is exited for radiation behavior problems. The modal input power P_{in} is determined by the MWC C_n, as shown in Eq. (14).

$$P_{in} = \frac{1}{2} \sum_n | C_n |^2$$ (14)

The above quantities explain how a design can succeed in the excitation of the desired modes.

Finally, this section summarizes the standard values for the measure of a resonant mode from the above parameters, i.e., eigenvalue (λ_n) = 0, MS = 1, and CA = 180°. They are essentially expressing the same thing differently, and which parameter is used depends on the personal design requirement. If the design requirement is only on the primary resonant mode or to identify a few lower-order resonant modes, the parameter extraction of the eigenvalue (λ_n) is sufficient. To extract the behavior of higher-order modes or over a wide frequency band of operation, MS is an important parameter. When multiple modes need to be excited for certain radiation performance (i.e., circular polarization), the CA and current or field distribution are of great importance in the antenna design.

3. CP Antennas Using CMA

CMA and its applications in antenna designs for enhancing various radiation parameters are described by various research groups in the literature. However, this section has limited the review to a parameter called circular polarization. The underlying mechanism of this parameter is readily available to be read through many electronic databases individually. This review process is highlighted, with all those approaches together, by classifying various groups based on the feed networks and the type of geometry. This will help further understand the insight into the design of the CP antenna and its ARBW enhancement using CMA.

Antenna polarization is usually defined as the orientation of an electric field as a function of time, at a fixed position in space. The polarization type of an antenna can be identified from the axial ratio (AR) [40-41]. If AR is zero or infinity, it is LP. For unity AR, it is circular polarization. If AR is between zero to one, it is elliptical polarization. However, for practical applications, the most acceptable AR is 1.414 = 3 dB for circular polarization.

To generate circular polarization in antennas, a well-known fact is to excite two orthogonal modes with equal amplitude and quadrature (90°) phase difference. Various techniques have been described in the literature using single- or dual-feeding techniques [42-43]. In a single-feeding method, a small perturbation is required for the orthogonal mode and a quadrature phase shift at the feed point. The perturbation segment is in the form of a slit, a slot, a truncated segment, or an added stub [44-46]. However, the single-feed antennas are structurally simple but suffer from narrow ARBW. To overcome this, a

dual-feed network is one of the solutions. However, dual-feed CP antennas require an additional power divider to split the input signal with equal amplitude and an additional quadrature wavelength transmission line to generate 90° phase shifts. This enhances the design complexity.

To compensate for the two issues, another type of CP antennas called slot and stub antennas has been proposed [47-49]. However, most of these antennas are usually accomplished by tuning the patch shapes and feed positions through full-wave simulation. Those designs have not been verified for the similarity between the natural resonance characteristics and the physical insight of the feed location. To address the above two characteristics and further optimization of the structure, CMA has been identified by many research groups. Using CMA and its parameter extraction, one can easily identify the circular polarization of the design from the following three conditions:

(1) The first condition to satisfy circular polarization is to identify adjacent orthogonal modes and this can be easily verified from the modal current distribution analysis for various modes.

(2) The next condition is that both orthogonal fields are with uniform magnitude and it can be verified from the MS between two orthogonal modes. If the MS is the same for two orthogonal modes at a certain frequency means, it satisfies the required condition.

(3) Finally, the last condition for circular polarization is a quadrature-phase difference between the modes and it can be verified from CA. If the CA difference between the orthogonal modes is 90° means, it satisfies the required condition.

With the use of the above three conditions, various CP antennas have been designed in the literature. These antennas mainly differ in the way by which the LP modes are excited properly with the help of CMA. To review those proposed structures, they are divided into two parts. The first part of the CP antennas is considered without metasurface (MTS) and the second part is with MTS.

3.1. CP antennas without MTS

To demonstrate how CMA is useful to achieve circular polarization, a simple rectangular asymmetrical U-shaped slot antenna as shown in Fig. 5 is considered [50]. CMA has been carried out without considering the feed structure. Fig. 6 shows the first two modes of MS and CA across the frequency band from 2.0-2.7 GHz. It is found that the two modes have the same large MS and a 90° phase difference at 2.3 GHz, which satisfies the above three conditions. As a result, for CP operations, these two modes operate together at the center frequency. Next, to find the optimal feed position, the characteristic currents as shown in Figs. 7(a) and (b) have been characterized in the horizontal mode and vertical mode with respect to the modes J_1 and J_2. Then, to excite two modes properly, the vertical mode is subtracted from the horizontal mode, i.e., performed $J_1 - J_2$ between the two modes. As a result, the minimum current has been obtained at the inner edge of the U-slot's long arm, as shown in Fig. 7(c). This location specifies that the two orthogonal modes represent a similar current amplitude. The two orthogonal modes that have comparable current density location points (indicated with the black dot in Fig. 5) will generate far-field CP radiation upon excitation.
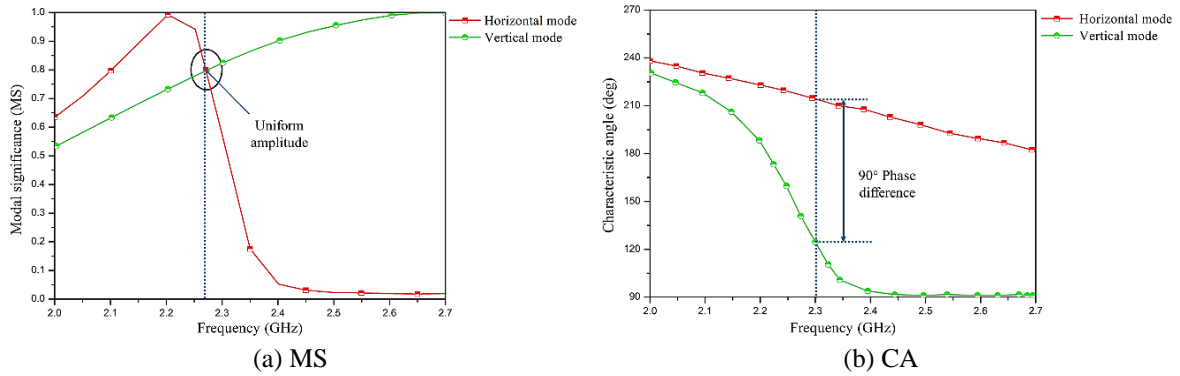
To generate the circular polarization, an equal current magnitude and 90° CA phase difference has been generated from an equal crossed dipole to an unequal crossed dipole [51]. It has been observed that a square contour parallel dipole has shown a 90° phase difference for degenerating modes such as mode 2 and mode 3 by analyzing individual orthogonal current modes [52]. The designs discussed above have a low profile and can be fabricated easily [53-59]. However, some of those structures exhibit a narrow ARBW because the orthogonality and phase difference is achieved at a single frequency.

To enhance the ARBW with a single-feed mechanism from CMA, Tran et al. [53.] coupled a higher band C-shaped monopole CP antenna with a lower band square patch with a C-shaped slot aperture, as shown in Fig. 8. To understand the ARBW enhancement, the MS, CA, current distribution, and far-field radiation of a C-shaped monopole and C-shaped slotted patch are presented in Fig. 9 and Fig. 10, respectively. As observed from Fig. 9, the first two modes are exactly the same, with a 90° phase difference at around 5.5 GHz radiating in a broadside direction. From Fig. 10, a similar phenomenon is observed for the first two

fundamental modes at around 2.1 GHz with broadside radiation. In addition, it is noticed that the same MS is quite close to 90° phase difference between the modes J_2 and J_4 as well as the modes J_2 and J_5 at 3.2 and 3.5 GHz, respectively. However, the current directions of the modes J_2 and J_4 are observed on the opposite side instead of having quadrature-phase differences. Hence, it has been considered that the C-shaped slotted patch is proposed to radiate CP waves at 2.1 and 3.5 GHz.
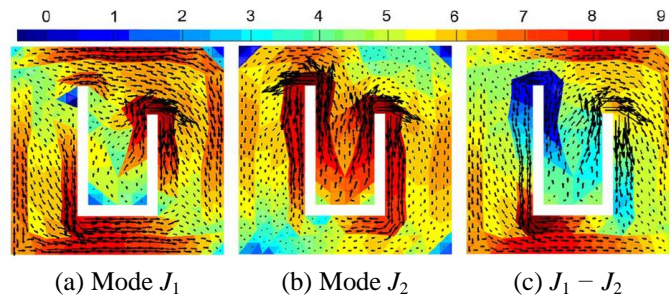

Fig. 5 Asymmetric U-slot antenna for circular polarization [50]

(a) MS   (b) CA

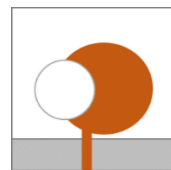Fig. 6 CM parameters of the asymmetric U-slot antenna [50]

(a) Mode J_1 (b) Mode J_2 (c) $J_1 - J_2$

Fig. 7 Current distribution of the U-slot antenna at 2.3 GHz [50]
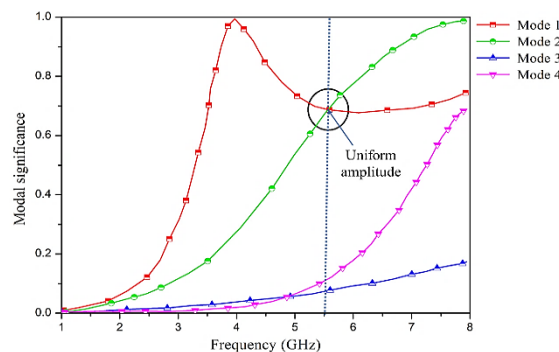

(a) Top layer   (b) Bottom layer

Fig. 8 Geometry of the CP C-shaped monopole antenna [53]

(a) MS

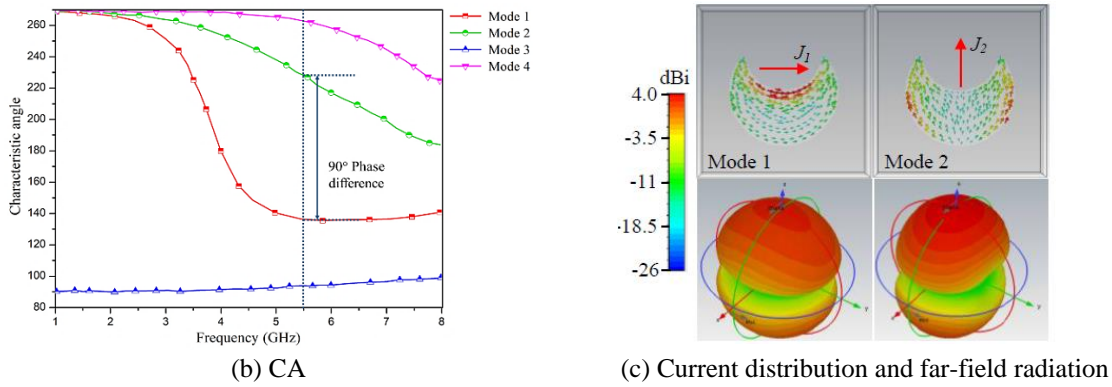Fig. 9 Modal characteristics of the C-shaped monopole patch [53]

(b) CA   (c) Current distribution and far-field radiation

Fig. 9 Modal characteristics of the C-shaped monopole patch [53] (continued)

(a) MS   (b) CA

(c) Far-field radiation

Fig. 10 Modal characteristics of the C-shaped slotted patch [53]

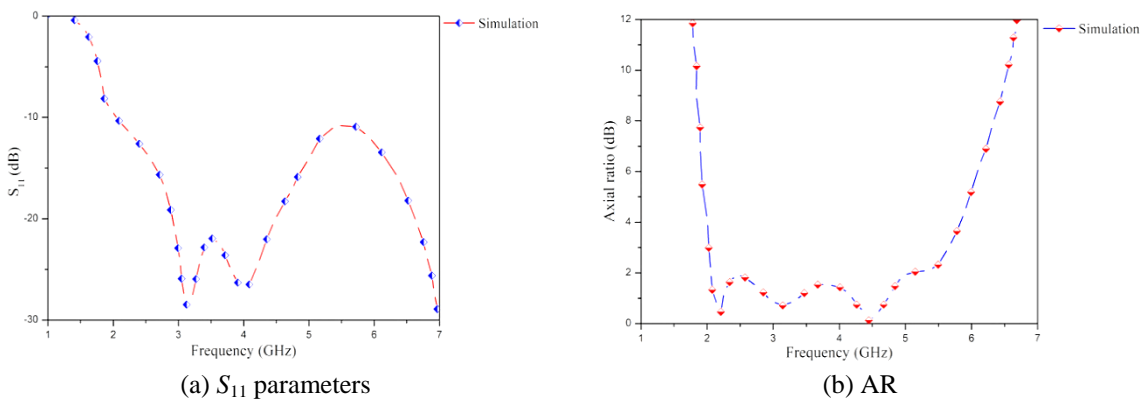(a) S_{11} parameters   (b) AR

Fig. 11 Parameters of the C-shaped monopole and C-shaped slotted patch antenna [53]

Once the desired modes have been selected for wide CP radiation from the above two shapes, the feed point from the C-shaped monopole patch is subsequently identified from the current distribution. It is identified as the feed point at the corner by subtracting the current mode J_2 from the mode J_1 of the C-shaped patch. Then, the patch is excited with a monopole arrangement and the ARBW is obtained ranging from 4.6 to 6.1 GHz. Next, to enhance the ARBW, the slotted C-shaped patch aperture is excited through a coupling mechanism with the directly fed C-shaped patch monopole. The final geometry of the CP antenna top and bottom layer design is shown in Fig. 10. Here, the CP radiation at 2.1 GHz and 3.5 GHz is predicted based on the desired

modes (J_1, J_2, and J_5) of the current distribution of the C-shaped slotted patch. Therefore, the position of the C-shaped patch monopole plays an extensive role in the performance of the C-slotted patch. To obtain the optimum coupling position, the design is fine-tuned using numerical simulation. The simulated S_{11} and ARBW results of an individual and optimized patch antenna are shown in Fig. 11. The results show that a very wide ARBW of 96.1% can be achieved in this configuration.

Using similar kinds of techniques, a CPW-fed rectangular slot antenna has been designed for wider ARBW [54-57]. The CP conditions are attained using an asymmetric slot [54] and asymmetric stubs [55] on the ground plane by altering the current distribution. Additionally, the ARBW has been improved by employing two symmetric inverted L-stubs with vertical strips parallel to an antenna and a pair of asymmetric inverted L-strips with spiral slots, respectively. In another design, a circular ring CPW-fed antenna has been proposed with two orthogonal clock angle microstrip lines on opposite sides of the substrate [56]. To attain a quadrature-phase difference CA, the angle between the microstrip lines is optimized to achieve circular polarization. Recently, a CP loop antenna has been designed with a broad ARBW and impedance bandwidth with a single-feeding technique [57]. Here, a 90° phase difference is attained by loading the lumped inductors. A pair of degenerated mode resonance points is split by properly positioning the feeds and loading the inductors with the aid of CMA. Using this method, an 8.3% ARBW and a 47% impedance bandwidth are achieved at 2.4 GHz WLAN band.

In summary, this subsection has reviewed the CMA of optimal antenna designs without MTS for CP radiation and improvement in AR. The optimal designs discussed above [55-57] demonstrate that CMA provides important information for CP performance and ARBW enhancement from CM parameters and current or field distribution. On the other hand, the designs described above illustrate how to optimize the feed position to provide CP radiation and improvement in ARBW from the modal current distribution.

3.2. CP antennas with MTS

This subsection investigates how CMA can be used to tailor the MTS for the purpose of designing CP antennas. Various MTSs are exploited in the CP radiation and ARBW improvement [58]. To demonstrate the usefulness of CMA with respect to MTS, the geometry of the MTS antenna is shown in Fig. 12. It comprises two dielectric layers and three metallic layers. The three metallic layers (i.e., the MTS, cross-shaped slot, and feed structure) are placed on the top, middle, and bottom of two substrates.

To analyze the CP behavior, CMA is first performed on the top MTS, and MS is demonstrated for the first four modes across the frequency band, as shown in Fig. 13(a). Then, the current distribution and far-field patterns of these modes at the respective resonance frequencies, such as 6 GHz (for the modes J_1 and J_2) and 6.5 GHz (for the modes J_3 and J_4), are observed as shown in Figs. 13(b) and (c). As observed from the modal currents, the modes J_1 and J_2 have an identical current distribution except for the 90° phase difference. However, they are a pair of degenerate modes and cannot provide 90° CA. The modes J_3 and J_4 are self-symmetrical modes with out-of-phase current distribution and appear null in the broadside direction. Hence, only mode 1 and mode 2 have been considered for CP radiation with simultaneous excitation with a 90° phase difference from the feed structure.

(a) Top view of MTS   (b) Cross slot   (c) Back view of the microstrip line
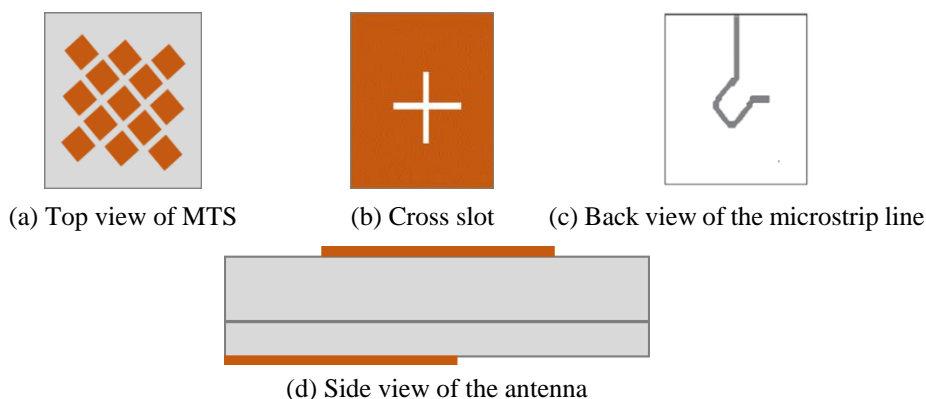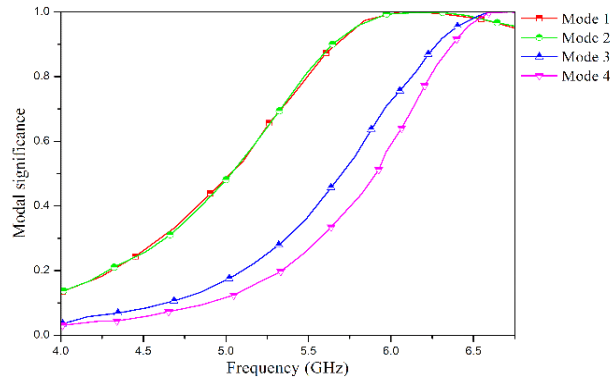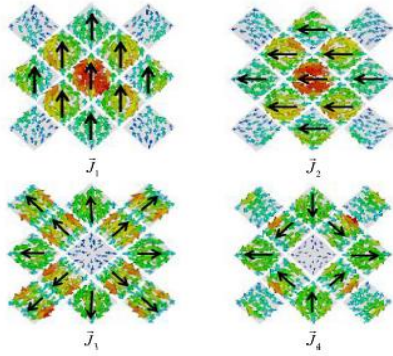
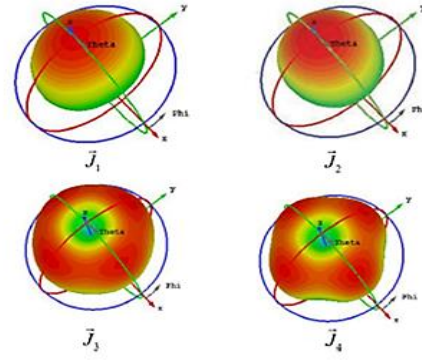(d) Side view of the antenna

Fig. 12 Configuration of the MTS-based antenna [58]
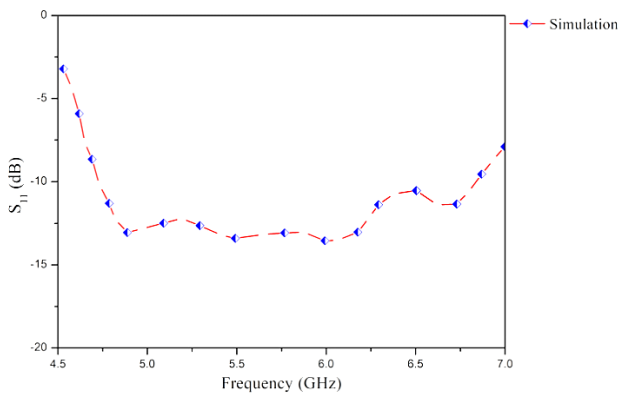
(a) MS

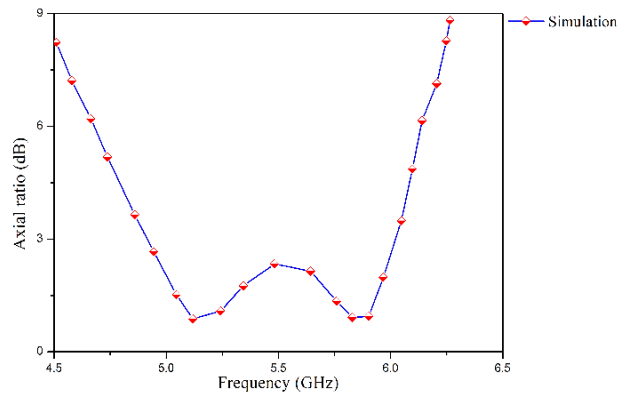(b) Current distribution   (c) Far-field patterns

Fig. 13 MTS CM parameters [58]

To excite only the first two modes with a 90° phase difference and suppress higher-order modes, an adaptive feed network has been employed with a combination of a cross-slot and a microstrip meander-line (Figs. 13(b) and (c)). As a result, CP radiation is formed. To investigate the CP performance, the S parameter and AR performance are compared in Fig. 14.

Further, various MTS antennas have been proposed in the literature based on the orthogonality principle of surface current distribution and identical MS between adjacent or lower-order modes and higher-order modes [59-62]. A perforated H-shaped MTS [59] and a corner-truncated patch MTS with capacitive loading strips [60] have been proposed by exciting adjacent higher-order modes and lower-order modes, respectively. Recently, another non-uniform Chebyshev distribution MTS has been exploited as a superstrate by exciting two alternative modes such as mode 1 and mode 3 with an equal electric field and relative phase difference close to 90° [61]. Apart from the ARBW enhancement, the CP MTS antenna has been proposed for radar cross-section (RCS) reduction [62]. Here, by using CMA, a linearly polarized slot antenna is converted to a CP antenna with the help of polarization-dependent MTS and is additionally used for RCS reduction. In another design, a dual CP MTS antenna has been proposed [63].

(a) S_{11} (b) AR

Fig. 14 MTS antenna parameters [58]

In this design, the desired modes are chosen and excited by a modified slot antenna with two orthogonal feeds. The modified cross slots, called two diagonal linear slot arms and a circular ring slot, introduce another resonance for wide ARBW. Apart from the ARBW enhancement, the MTS is also used for polarization conversion [64]. Here, various etching mechanisms, like diagonal slot, cross slot, and corner truncation, have been used on a linearly polarized rectangular MTS. To achieve circular polarization, this has been done with the exciting slot antenna. Modal analysis is used to verify CP conditions and optimize them. Recently, an artificial magnetic conductor (AMC)-based reflector CP antenna using a CPW-fed structure has been proposed for 5G sub-6 GHz communications with unidirectional radiation [65]. The periodic metallic square patches AMC improve ARBW from 27.27% to 51.67% and gain increases from 3.3 dBic to 8.7 dBic than the conventional PEC.

From the above discussion, it can be summarized that orthogonality is verified before the selection of a specific feed design. If any of the CP conditions are not satisfied for a simultaneous 90° phase difference for excitation, it has been optimized from the feed network and further analyzed. In some designs, the quadrature phase shift has not been attained from the CMA and has been compensated by properly designing the feed network. Moreover, the largest MS of different modes at the same frequency and different frequencies together with the 90° phase differences can generate narrowband and wideband ARBW, respectively. Studies have also indicated how to optimize CP antenna designs for two linear modes using MTS. After identifying the CP waves in a particular frequency band with the CMA, antenna designers concentrate their effort on the feed structure.

Moreover, in the literature, most of the CMA has been carried out for isolated patches by neglecting the ground plane and dielectric material. The accuracy of the resonant frequencies will be affected by such kind of simplification. This is because the characteristic fields and currents are dependent on the size and shape of the patch as well as the dielectric substrate. Hence, while considering CMA, the dielectric substrate and ground plane cannot be ignored when seeking resonant frequencies of microstrip antennas. Moreover, Fig. 15 represents a potential MTS utilized for circular polarization and ARBW enhancement using CMA.

Additionally, the design approaches discussed above are consolidated in Fig. 16 based on the utilized feed network. Moreover, the analysis of these parameters is performed before the selection of source excitation. Thus, there is a degree of freedom in the feed network selection and feed location in the final antenna design. Therefore, the techniques for the selection of feed networks and their final optimization with the help of CMA are reviewed in the above section from the mentioned literature [50-65]. Fig. 17 shows the antenna designs for various feeding methods. Additionally, the important observations of all these antenna designs are summarized with their achieved operating band and ARBW as shown in Table 1.
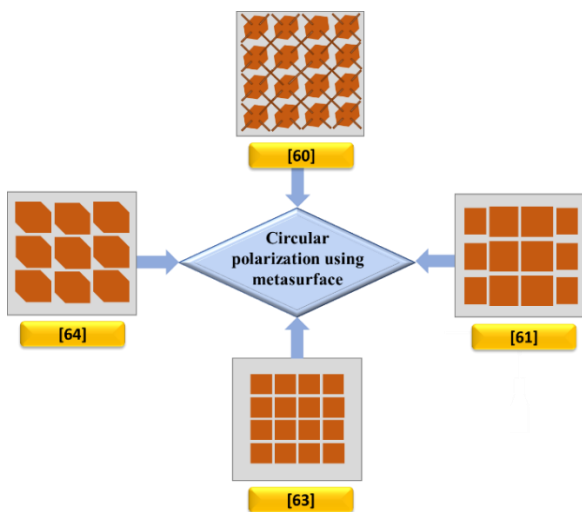

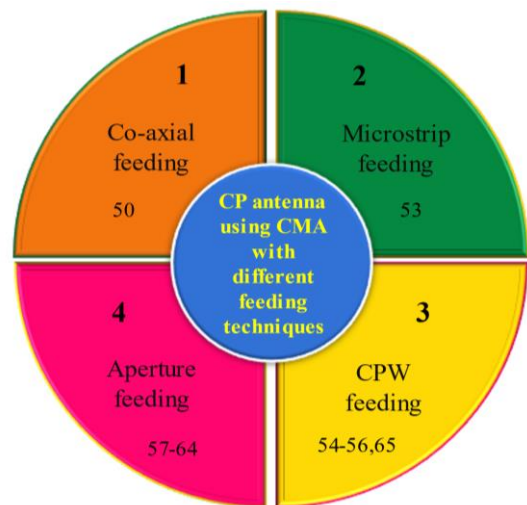Fig. 15 Typical MTS geometry utilized for circular polarization using CMA

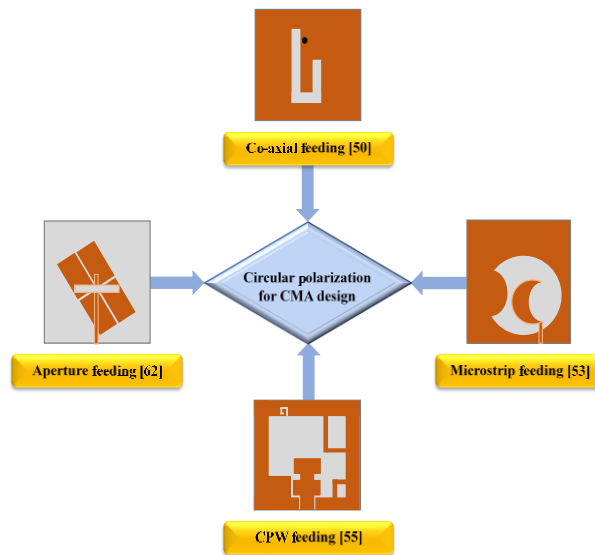Fig. 16 CP antennas designed using CMA with different feeding techniques

Fig 17 Typical CP geometry using CMA with various feeding methods

Table 1 Summary on various antenna design approaches for circular polarization

Ref.	Antenna design approach	AR band (GHz)	ARBW (% and GHz)	Gain (dBi)	Observation
[50]	(a) An asymmetric U-slot antenna (b) A redundant E-slot antenna	(a) 2.28-2.37 (b) 2.2-2.55	(a) 3.8 and 0.09 (b) 3.7 and 0.35	(a) 5.86 (b) 8.87	(a) An offset probe feed provides better AR performance than a center feed. (b) An insignificant mode is suppressed to get a redundant E-shaped slot antenna.
[51]	Two crossed-dipole antennas	0.282-0.295.5	4.65 and 13.5	-	The length of one dipole is increased slightly to get a 90° phase shift.
[54]	A small semicircular slot rectangular antenna	2.25-4.4	64.6 and 2.15	-	The inverted-L stubs are used for desired phase difference and diagonal corner truncation for orthogonal modes.
[55]	An I-shaped radiating patch	6.6-11.8	56.5 and 5.2	5.5	The simultaneous excitation of even and odd modes from a rectangular stub, inverted-L stub, and spiral slot provides the wideband radiation behavior.
[56]	A clock-shaped antenna from a metallic ring antenna	2.38-5.8	84.6 and 3.42	3.9	A 90° phase difference is introduced by the two opposite microstrip lines in the X and Y directions.
[59]	A crossed shape aperture with H-shaped unit cell MTS	5.2-6	14.3 and 0.8	9.4	The additional required phase for circular polarization is compensated via a cross-shaped strip with an aperture.
[60]	A corner-truncated patch along with a pair of inserted capacitive loading strips	3.3-3.6	8.5 and 0.3	6.57	From CMA, the pair of inserted diagonal capacitive loading strips of a corner-truncated patch is optimized for attaining quadrature phase difference and ARBW improvement.
[61]	A non-uniform MTS superstrate layer excited by a stripline through a rectangular slot	1.99-2.37	17.4 and 0.265	7.1-8	The phase difference between the orthogonal modes is observed only 60° and exploited as an inductive exciter for an additional 30° phase shift.
[62]	A rectangular patch as a polarization-dependent MTS	5.83-6.32	9.05 and 0.49	6.4	The degenerated modes are achieved using polarization-dependent MTS with 74° phase difference and excited with a linearly polarized slot antenna to achieve CP radiation.
[63]	An MTS excited with a hybrid feed system consisting of a cross slot and a microstrip line	2.15-2.95	31.3 and 0.8	7.01	Due to a cross-slot on the ground plane, 90° phase difference is presented via microstrip meander line excitation.
[64]	A square patch with a diagonal slot, crossed slot, and corner-truncated MTS	2.32-2.46 2.55-2.58 2.52-2.54	5.8 and 0.14 1.1 and 0.03 0.7 and 0.02	5 3.5 3.5	Due to asymmetry on the square patch, a phase difference is created for circular polarization.

4. Conclusions

This article concentrated on modal parameters that are required to analyze the natural mode resonance and radiating behavior, followed by a novel approach for designing an antenna using CMA to improve ARBW. The CM parameters together with characteristic currents explicitly gave useful information for analysis of the antenna before excitation. In particular, this review

presented how the ARBW is enhanced in various developed structures from the theoretical formation analysis of the CM theory. The information provided by these developed structures helps understand valuable insights for the selection of feed position to maximize the antenna performance. Moreover, the authors' abundant contributions to the study of the CM theory were summarized based on the feed structures, utilizing MTS with concluding remarks. Fully exploiting and making use of CMA in antenna designs could significantly enhance 5G and mm-wave applications from the dual-polarized CP antenna perspective.

From a future perspective, if CP antennas can fulfill the needs of long-distance communication as done by high gain linearly polarized antennas, the CM-based approach becomes attractive in antenna designs. Numerical models, physical interpretation insights, and CMA would be available for a more detailed analysis of CP antennas with and without MTS. This approach is also helpful to demonstrate that simultaneous MIMO operations increase channel capacity and throughput. For efficient MIMO performance, the radiation diversity is also explored for its low correlation coefficient. Additionally, further research is going on to improve other important parameters, such as gain, efficiency, compactness, and polarization purity. Finally, these challenges require the CMA method to become more efficient for designing CP antennas.

Conflicts of Interest

The authors declare no conflict of interest.

References

[1] R. S. Uqaili, J. A. Uqaili, S. Zahra, F. B. Soomro, and A. Akbar, "A Study on Dual-Band Microstrip Rectangular Patch Antenna for Wi-Fi," Proceedings of Engineering and Technology Innovation, vol. 16, pp. 1-12, August 2020.

[2] S. Patil, V. Kapse, S. Sharma, and A. K. Pandey, "Low Profile Wideband Dual-Ring Slot Antenna for Biomedical Applications," Proceedings of Engineering and Technology Innovation, vol. 19, pp. 38-44, August 2021.

[3] V. Kollipara, S. Peddakrishna, and J. Kumar, "Planar EBG Loaded UWB Monopole Antenna with Triple Notch Characteristics," International Journal of Engineering and Technology Innovation, vol. 11, no. 4, pp. 294-304, September 2021.

[4] A. Kumar and A. P. S. Pharwaha, "Design and Optimization of Micro-Machined Sierpinski Carpet Fractal Antenna Using Ant Lion Optimization," International Journal of Engineering and Technology Innovation, vol. 10, no. 4, pp. 306-318, September 2020.

[5] K. A. Khan and S. M. Nokerov, "Optimization of Multi-Band Characteristics in Fan-Stub Shaped Patch Antenna for LTE (CBRS) and WLAN Bands," Proceedings of Engineering and Technology Innovation, vol. 18, pp. 25-35, April 2021.

[6] S. S. Gao, Q. Luo, and F. Zhu, Circularly Polarized Antennas, UK: IEEE Press, 2013.

[7] R. Zenter, Z. Sipus, and J. Bartolic, "Optimization Synthesis of Broadband Circularly Polarized Microstrip Antennas by Hybrid Genetic Algorithm," Microwave and Optical Technology Letters, vol. 31, no. 3, pp. 197-201, November 2001.

[8] R. L. Haupt, "Antenna Design with a Mixed Integer Genetic Algorithm," IEEE Transactions on Antennas and Propagation, vol. 55, no. 3, pp. 577-582, March 2007.

[9] Y. Chen and C. F. Wang, Characteristic Modes: Theory and Applications in Antenna Engineering, Hoboken: Wiley, 2015.

[10] B. Yang and J. J. Adams, "Computing and Visualizing the Input Parameters of Arbitrary Planar Antennas via Eigenfunctions," IEEE Transactions on Antennas and Propagation, vol. 64, no. 7, pp. 2707-2718, July 2016.

[11] B. B. Q. Elias, P. J. Soh, A. A. Al-Hadi, P. Akkaraekthalin, and G. A. Vandenbosh, "A Review of Antenna Analysis Using Characteristic Modes," IEEE Access, vol. 9, pp. 98833-98865, July 2021.

[12] R. J. Garbacz, "Modal Expansions for Resonance Scattering and Phenomena," Proceedings of the IEEE, vol. 53, no. 8, pp. 856-864, August 1965.

[13] R. Garbacz and R. Turpin, "A Generalized Expansion for Radiated and Scattered Fields," IEEE Transactions on Antennas and Propagation, vol. 19, no. 3, pp. 348-358, May 1971.

[14] R. Harrington and J. Mautz, "Theory of Characteristic Modes for Conducting Bodies," IEEE Transactions on Antennas and Propagation, vol. 19, no. 5, pp. 622-628, September 1971.

[15] E. Safin and D. Manteuffel, "Reconstruction of the Characteristic Modes on an Antenna Based on the Radiated Far Field," IEEE Transactions on Antennas and Propagation, vol. 61, no. 6, pp. 2964-2971, June 2013.

[16] T. Bernabeu-Jiménez, A. Valero-Nogueira, F. Vico-Bondia, E. Antonino-Daviu, and M. Cabedo-Fabres, "A 60-GHz LTCC Rectangular Dielectric Resonator Antenna Design with Characteristic Modes Theory," IEEE Antennas and Propagation Society International Symposium, pp. 1928-1929, July 2014.

[17] R. T. Maximidis, C. L. Zekios, T. N. Kaifas, E. E. Vafiadis, and G. A. Kyriacou, "Characteristic Mode Analysis of Composite Metal-Dielectric Structure Based on Surface Integral Equation/Moment Method," 8th European Conference on Antennas and Propagation, pp. 2822-2826, April 2014.

[18] H. Alroughani, J. Ethier, and D. A. McNamara, "Observations on Computational Outcomes for the Characteristic Modes of Dielectric Objects," IEEE Antennas and Propagation Society International Symposium, pp. 844-845, July 2014.

[19] Y. Chen and C. F. Wang, "Surface Integral Equation Based Characteristic Mode Formulation for Dielectric Resonators," IEEE Antennas and Propagation Society International Symposium, pp. 846-847, July 2014.

[20] Z. Miers, H. Li, and B. K. Lau, "Design of Bezel Antennas for Multiband MIMO Terminals Using Characteristic Modes," 8th European Conference on Antennas and Propagation, pp. 2556-2560, April 2014.

[21] R. Rezaiesarlak and M. Manteghi, "On the Application of Characteristic Modes for the Design of Chipless RFID Tags," IEEE Antennas and Propagation Society International Symposium, pp. 1304-1305, July 2014.

[22] E. A. Elghannai and R. G. Rojas, "Design of USB Dongle Antenna for WLAN Applications Using Theory of Characteristic Modes," Electronics Letters, vol. 50, no. 4, pp. 249-251, February 2014.

[23] J. Chalas, K. Sertel, and J. L. Volakis, "NVIS Synthesis for Electrically Small Aircraft Using Characteristic Modes," IEEE Antennas and Propagation Society International Symposium, pp. 1431-1432, July 2014.

[24] A. Krewski, "2-Port MIMO Antenna System for High Frequency Data Link with UAVs Using Characteristic Modes," IEEE Antennas and Propagation Society International Symposium, pp. 364-365, July 2013.

[25] Y. Chen and C. F. Wang, "Electrically Small UAV Antenna Design Using Characteristic Modes," IEEE Transactions on Antennas and Propagation, vol. 62, no. 2, pp. 535-545, February 2014.

[26] Y. Chen and C. F. Wang, "Shipboard NVIS Radiation System Design Using the Theory of Characteristic Modes," IEEE Antennas and Propagation Society International Symposium, pp. 852-853, July 2014.

[27] B. A. Austin and K. P. Murray, "The Application of Characteristic-Mode Techniques to Vehicle-Mounted NVIS Antennas," IEEE Antennas and Propagation Magazine, vol. 40, no. 1, pp. 7-21, February 1998.

[28] K. P. Murray and B. A. Austin, "Synthesis of Vehicular Antenna NVIS Radiation Patterns Using the Method of Characteristic Modes," IEE Proceedings—Microwaves, Antennas, and Propagation, vol. 141, no. 3, pp. 151-154, June 1994.

[29] M. Ignatenko and D. Filipovic, "Application of Characteristic Mode Analysis to HF Low Profile Vehicular Antennas," IEEE Antennas and Propagation Society International Symposium, pp. 850-851, July 2014.

[30] A. Mohanty and B. R. Behera. "Characteristics Mode Analysis: A Review of Its Concepts, Recent Trends, State-of-the-Art Developments and Its Interpretation with a Fractal UWB MIMO Antenna," Progress in Electromagnetics Research B, vol. 92, pp. 19-45, March 2021.

[31] A. Mohanty and B. R. Behera, "CMA Assisted 4-Port Compact MIMO Antenna with Dual-Polarization Characteristics," AEÜ —International Journal of Electronics and Communications, vol. 137, Article no. 153794, May 2021.

[32] A. H. Jabire, H. X. Zheng, A. Abdu, and Z. Song, "Characteristic Mode Analysis and Design of Wide Band MIMO Antenna Consisting of Metamaterial Unit Cell," Electronics, vol. 8, no. 1, Article no. 68, January 2019.

[33] T. Li and Z. N. Chen, "Design of Dual Band Metasurface Antenna Array Using Characteristic Mode Analysis (CMA) for 5G Millimeter-Wave Applications," IEEE-APS Topical Conference on Antennas and Propagation in Wireless Communications, pp. 721-724, September 2018.

[34] B. Feng, X. He, J. Cheng, and C. Sim, "Dual-Wideband Dual-Polarized Metasurface Antenna Array for the 5G Millimeter Wave Communications Based on Characteristic Mode Theory," IEEE Access, vol. 8, pp. 21589-21601, January 2020.

[35] K. Gao, X. Ding, L. Gu, Y. Zhao, and Z. Nie, "A Broadband Dual Circularly Polarized Shared-Aperture Antenna Array Using Characteristic Mode Analysis for 5G Applications," International Journal of RF and Microwave Computer-Aided Engineering, vol. 31, no. 3, Article no. e22539, March 2021.

[36] A. Abdelaziz, H. A. Mohamed, and E. K. Hamad, "Applying Characteristic Mode Analysis to Systematically Design of 5G Logarithmic Spiral MIMO Patch Antenna," IEEE Access, vol. 9, pp. 156566-156580, November 2021.

[37] A. Kishk and L. Shafai, "Different Formulations for Numerical Solution of Single or Multibodies of Revolution with Mixed Boundary Conditions," IEEE Transactions on Antennas and Propagation, vol. 34, no. 5, pp. 666-673, May 1986.

[38] A. Sharif, J. Ouyang, F. Yang, R. Long, and M. K. Ishfaq, "Tunable Platform Tolerant Antenna Design for RFID and IoT Applications Using Characteristic Mode Analysis," Wireless Communications and Mobile Computing, vol. 2018, Article no. 9546854, 2018.

[39] R. Martens, E. Safin, and D. Manteuffel, "Inductive and Capacitive Excitation of the Characteristic Modes of Small Terminals," Loughborough Antennas and Propagation Conference, pp. 1-4, November 2011.

[40] C. A. Balanis, Antenna Theory: Analysis and Design, 3rd ed., New Jersey: John Wiley & Sons, 2005.

[41] Y. Dong, H. Toyao, and T. Itoh, "Compact Circularly-Polarized Patch Antenna Loaded with Metamaterial Structures," IEEE Transactions on Antennas and Propagation, vol. 59, no. 11, pp. 4329-4334, November 2011.

[42] J. S. Row and C. Y. Ai, "Compact Design of Single-Feed Circularly Polarized Microstrip Antenna," Electronics Letters, vol. 40, no. 18, pp. 1093-1094, September 2004.

[43] Q. Zhu, S. Yang, and Z. Chen, "Modified Corner-Fed Dual Polarised Stacked Patch Antenna for Micro-Base Station Applications," Electronics Letters, vol. 51, no. 8, pp. 604-606, April 2015.

[44] J. Y. Sze and C. C. Chang, "Circularly Polarized Square Slot Antenna with a Pair of Inverted-L Grounded Strips," IEEE Antennas and Wireless Propagation Letters, vol. 7, pp. 149-151, March 2008.

[45] Y. Sung, "Axial Ratio-Tuned Circularly Polarized Square Patch Antenna with Long Stubs," International Journal of Antennas and Propagation, vol. 2018, Article no. 7068560, 2018.

[46] C. F. Zhou and S. W. Cheung, "A Wideband CP Crossed Slot Antenna Using 1-λ Resonant Mode with Single Feeding," IEEE Transactions on Antennas and Propagation, vol. 65, no. 8, pp. 4268-4273, August 2017.

[47] C. Y. D. Sim, H. D. Chen, and L. Zuo, "CPW-Fed Square Ring Slot Antenna with Circular Polarization Radiation for Wimax/WLAN Applications," Microwave and Optical Technology Letters, vol. 57, no. 4, pp. 886-891, February 2015.

[48] S. Dentri, C. Phongcharoenpanich, and K. Kaemarungsi, "Single-Fed Broadband Circularly Polarized Unidirectional Antenna Using Folded Plate with Parasitic Patch for Universal UHF RFID Readers," International Journal of RF Microwave Computer-Aided Engineering, vol. 26, no. 7, pp. 575-587, September 2016.

[49] S. B. Vignesh, Nasimuddin, and A. Alphones, "Stubs-Integrated-Microstrip Antenna Design for Wide Coverage of Circularly Polarised Radiation," IET Microwaves, Antennas, and Propagation, vol. 11, no. 4, pp. 444-449, September 2016.

[50] Y. Chen and C. F. Wang, "Characteristic-Mode-Based Improvement of Circularly Polarized U-Slot and E-Shaped Patch Antennas," IEEE Antennas and Wireless Propagation Letters, vol. 11, pp. 1474-1477, November 2012.

[51] J. P. Ciafardini, E. A. Daviu, M. C. Fabrés, N. M. M. Hicho, J. A. Bava, and M. F. Bataller, "Analysis of Crossed Dipole to Obtain Circular Polarization Applying Characteristic Modes Techniques," IEEE Biennial Congress of Argentina, pp. 1-5, June 2016.

[52] J. F. Lin and Q. X. Chu, "A Modal Approach to Evaluating the Axial Ratio of Circularly Polarized Antennas," IEEE International Conference on Computational Electromagnetics, pp. 202-204, February 2016.

[53] H. H. Tran, N. Nguyen-Trong, and A. M. Abbosh, "Simple Design Procedure of a Broadband Circularly Polarized Slot Monopole Antenna Assisted by Characteristic Mode Analysis," IEEE Access, vol. 6, pp. 78386-78393, 2018.

[54] K. Saraswat and A. R. Harish, "Analysis of Wideband Circularly Polarized Ring Slot Antenna Using Characteristics Mode for Bandwidth Enhancement," International Journal of RF and Microwave Computer-Aided Engineering, vol. 28, no. 2, Article no. e21186, September 2017.

[55] M. M. S. Jaiverdhan, R. P. Yadav, and R. Dhara, "Characteristic Mode Analysis and Design of Broadband Circularly Polarized CPW-Fed Compact Printed Square Slot Antenna," Progress in Electromagnetics Research M, vol. 94, pp. 105-118, July 2020.

[56] M. Han and W. Dou, "Compact Clock-Shaped Broadband Circularly Polarized Antenna Based on Characteristic Mode Analysis," IEEE Access, vol. 7, pp. 159952-159959, November 2019.

[57] Y. Chen, X. Li, Z. Qi, H. Zhu, and S. Zhao, "A Single-Feed Circularly Polarized Loop Antenna Using Characteristic Mode Analysis," International Journal of RF and Microwave Computer-Aided Engineering, vol. 31, no. 7, Article no. e22648, July 2021.

[58] X. Gao, G. Tian, Z. Shou, and S. Li, "A Low-Profile Broadband Circularly Polarized Patch Antenna Based on Characteristic Mode Analysis," IEEE Antennas and Wireless Propagation Letters, vol. 20, no. 2, pp. 214-218, December 2020.

[59] C. Zhao and C. F. Wang, "Characteristic Mode Design of Wide Band Circularly Polarized Patch Antenna Consisting of H-Shaped Unit Cells," IEEE Access, vol. 6, pp. 25292-25299, 2018.

[60] Y. Juan, W. Yang, and W. Che, "Miniaturized Low-Profile Circularly Polarized Metasurface Antenna Using Capacitive Loading," IEEE Transactions on Antennas and Propagation, vol. 67, no. 5, pp. 3527-3532, May 2019.

[61] F. A. Dicandia and S. Genovesi, "Characteristic Modes Analysis of Non-Uniform Metasurface Superstrate for Nanosatellite Antenna Design," IEEE Access, vol. 8, pp. 176050-176061, 2020.

[62] P. K. Rajanna, K. Rudramuni, and K. Kandasamy, "Characteristic Mode-Based Compact Circularly Polarized Metasurface Antenna for In-Band RCS Reduction," International Journal of Microwave and Wireless Technologies, vol. 12, no. 2, pp. 131-137, March 2020.

[63] S. Liu, D. Yang, and J. Pan, "A Low-Profile Broadband Dual-Circularly-Polarized Metasurface Antenna," IEEE Antennas and Wireless Propagation Letters, vol. 18, no. 7, pp. 1395-1399, July 2019.

[64] P. V. Kumar and B. Ghosh, "Characteristic Mode Analysis of Linear to Circular Polarization Conversion Metasurface," Electromagnetics, vol. 40, no. 8, pp. 605-612, March 2020.

[65] H. Askari, N. Hussain, D. Choi, M. A. Sufian, A. Abbas, and N. Kim, "An AMC-Based Circularly Polarized Antenna for 5G Sub-6 GHz Communications," Computers, Materials, and Continua, vol. 69, no. 3, pp. 2997-3013, August 2021.